

27 **Abstract**

28 The Global atmospheric Electric Circuit (GEC) is a fundamental coupling network of the climate
29 system connecting electrically disturbed weather regions with fair weather regions across the
30 planet. The GEC sustains the fair weather electric field (or potential gradient, PG) which is
31 present globally and can be measured routinely at the surface using durable instrumentation
32 such as modern electric field mills, which are now widely deployed internationally. In contrast to
33 lightning or magnetic fields, fair weather PG cannot be measured remotely. Despite the
34 existence of many PG datasets (both contemporary and historical), few attempts have been
35 made to coordinate and integrate these fragmented surface measurements within a global
36 framework. Such a synthesis is important in order to fully study major influences on the
37 GEC such as climate variations and space weather effects, as well as more local atmospheric
38 electrical processes such as cloud electrification, lightning initiation, and dust and aerosol
39 charging.

40

41 The GloCAEM (Global Coordination of Atmospheric Electricity Measurements) project has
42 brought together experts in atmospheric electricity to make the first steps towards an effective
43 global network for atmospheric electricity monitoring, which will provide data in near real time.
44 Data from all sites are available in identically-formatted files, at both one second and one minute
45 temporal resolution, along with meteorological data (wherever available) for ease of
46 interpretation of electrical measurements. This work describes the details of the GloCAEM
47 database and presents what is likely to be the largest single analysis of PG data performed from
48 multiple datasets at geographically distinct locations. Analysis of the diurnal variation in PG
49 from all 17 GloCAEM sites demonstrates that the majority of sites show two daily maxima,
50 characteristic of local influences on the PG, such as the sunrise effect. Data analysis methods
51 to minimise such effects are presented and recommendations provided on the most suitable
52 GloCAEM sites for the study of various scientific phenomena. The use of the dataset for a

53 further understanding of the GEC is also demonstrated, in particular for more detailed
54 characterization of day-to-day global circuit variability. Such coordinated effort enables deeper
55 insight into PG phenomenology which goes beyond single-location PG measurements,
56 providing a simple measurement of global thunderstorm variability on a day-to-day timescale.
57 The creation of the GloCAEM database is likely to enable much more effective study of
58 atmospheric electricity variables than has ever been possible before, which will improve our
59 understanding of the role of atmospheric electricity in the complex processes underlying
60 weather and climate.

61

62 1. Introduction

63 Earth's electrical environment has been studied since the 1750s, but its more recently-
64 appreciated connections to clouds (Tinsley et al, 2007, Nicoll and Harrison, 2016) and climate
65 (Price, 1993; Rycroft et al, 2000; Williams, 1992; Williams, 2005) have highlighted some
66 incompleteness in understanding of atmospheric electricity in the climate system. It is well
67 established that Earth has a "Global atmospheric Electric Circuit" (GEC), through which charge
68 separation in thunderstorms sustains large scale current flow around the planet (Wilson, 1921;
69 Williams, 2009). The GEC sustains the fair weather (FW) electric field (or potential gradient,
70 PG, as it is also known¹), which is present globally in regions which are not strongly electrically
71 disturbed by weather or aerosol. In such conditions, the PG can be related to the local electrical
72 conductivity of air, σ , through Ohm's Law:

$$73 \qquad \qquad \qquad PG = -\frac{J_c}{\sigma} \qquad \qquad \qquad (1)$$

74 where J_c is the air-Earth conduction current which flows vertically from the ionosphere to Earth's
75 surface. Provided no local charge separation processes are active, J_c can be considered
76 constant, hence the PG is inversely proportional to σ , and any phenomena (such as
77 meteorological processes like fog or aerosol pollution) which perturb σ will also affect the PG.
78 PG can be measured routinely using well-established electric field mill instrumentation (e.g.
79 Nicoll 2012). Measurements of PG can contribute to our understanding of how thunderstorms
80 and the global atmospheric electrical system may be varying within our changing climate, which
81 are difficult to assess by global lightning networks because they are not stable with time. PG
82 measurements are also useful in understanding some of the fundamental processes occurring
83 inside thunderstorms which are only just starting to be understood such as high energy particle
84 emissions related to thunderstorm ground enhancements (TGEs) and terrestrial gamma ray
85 flashes (TGFs) (e.g. Chilingarian et al, 2015; Chilingarian, 2018). However, in order that truly

¹ By convention, PG is the negative of the electric field. Hence, in fair weather, when the atmospheric electric field is negative, the PG is therefore positive.

86 global signals are considered in understanding the processes within the global circuit, many
87 validating measurements must be made simultaneously at different locations around the world.

88

89 Beyond thunderstorms, another area of current research in atmospheric electricity is the role
90 that atmospheric electricity plays in modulating cloud properties and therefore its indirect effects
91 through clouds on the Earth's radiative balance. Recent evidence demonstrates that all
92 persistent extensive layer clouds are electrically charged at their upper and lower boundaries,
93 which theory indicates can influence cloud microphysical processes (Nicoll and Harrison, 2016).
94 Since layer clouds are common globally, electrical effects on cloud microphysics may therefore
95 always be contributing some of the underlying variability in cloud properties. One of the most
96 uncertain elements is the effect of space weather influences on atmospheric electricity, through
97 lower atmosphere changes in cosmic ray ionisation from solar flares and energetic particle
98 events. Recent work (e.g. Michnowski, 1998; Harrison et al, 2013; Smirnov, 2014) has reported
99 effects of space weather influences on the PG at individual sites, but in order to identify and
100 understand global effects, simultaneous measurements are required at multiple locations.

101

102 Despite the central role of lightning as a weather hazard and the potentially widespread
103 importance of charge for many atmospheric processes involving particles and droplets, research
104 is hampered by the fragmented nature of surface atmospheric electricity measurements, making
105 anything other than local studies in fortuitous FW conditions difficult. In contrast to detection of
106 global lightning using satellite-carried instruments and ground-based radio networks, fair
107 weather PG cannot be measured by remote sensing and no similar extensive measurement
108 networks exist for its study. This has been a major limitation on research into FW atmospheric
109 electricity. Some valuable regional PG monitoring networks have however been established,
110 such as at NASA Kennedy Space Centre (e.g. Krider, 1989; Lucas et al, 2017); in the Russian
111 Federation (Shvarts et al, 2008) and in South America (AFINSA) (Raulin et al, 2014; Tacza et

112 al, 2014), but these cover only a small part of Earth's surface. Archiving of historical
113 atmospheric electrical data has also been achieved by the ATMEL2007A database (Tammet,
114 2009) which compiled a large number of hourly datasets from Russia and Europe. These
115 valuable datasets are now historical, as data is only most recently available up to 2006. There is
116 now an opportunity to widen the geographical coverage of available PG measurements as many
117 researchers worldwide currently make high temporal resolution measurements of the FW PG
118 routinely, which is neither coordinated nor exploited. The UK-led GloCAEM (Global Coordination
119 of Atmospheric Electricity) project has brought these experts together to make the first steps
120 towards an effective global network for FW atmospheric electricity monitoring, with publicly
121 available data and in near real time. Another novel aspect of the GloCAEM dataset is the
122 availability of meteorological data alongside the PG measurements. The meteorological
123 information is, firstly, central in independently determining the existence of fair weather
124 conditions (due to the substantial influence of non-fair weather meteorological phenomena on
125 the PG), which are required to study global and space weather influences on the PG, and,
126 secondly useful in allowing study of the effect of variations in local meteorology on the electrical
127 environment. The use of identical format files for each GloCAEM measurement site makes data
128 analysis, in particular comparison of data from all the sites, very straightforward, which is a key
129 aspect of the project in driving research in atmospheric electricity forward.

130

131 This paper describes the properties of the GloCAEM database, as well as presents a summary
132 of some of the initial analysis performed with the dataset. This focuses on the application of the
133 data to Global Electric Circuit research, but also provides advice on choice of the best
134 GloCAEM sites at which to study a variety of different atmospheric and geophysical processes
135 related to atmospheric electricity.

136

137 **2. The GloCAEM dataset**

138 **2.1 Overview**

139 The GloCAEM dataset so far contains PG and meteorological data from 12 different
140 international institutions and 17 different locations worldwide. It is stored at the UK Centre for
141 Environmental Data Analysis (CEDA), which is a Data Repository funded by several of the UK
142 research councils (<http://www.ceda.ac.uk/>). CEDA provides secure and long term storage of
143 datasets for atmospheric research for the academic community. The GloCAEM dataset will
144 therefore become publicly available (with users registering for a username and password
145 through CEDA) for research use when the period of data checking is completed, with the
146 functional launch expected to be from summer 2019. Some key details of the GloCAEM dataset
147 functionality are listed below:

148

- 149 - Data values are provided in as close to real time as possible (at sites where internet and
150 FTP are available),
- 151 - Data files are provided as daily files, at two different time resolutions: 1 second and
152 1 minute averages,
- 153 - Data files of 1 second resolution contain only PG data; 1 minute files contain PG and
154 meteorological data at the same temporal resolution (where available)
- 155 - Downloadable site information and instrument information files are provided for each
156 location at the project website ([https://glocaem.wordpress.com/introduction/project-
157 partners-and-measurement-sites/](https://glocaem.wordpress.com/introduction/project-partners-and-measurement-sites/)).

158

159 The use of daily data files allows the user to choose whether to download only a few files if
160 analysing one specific event, or the entire dataset. The GloCAEM sites are essentially a virtual
161 network in that the network has not specifically been created to provide new sites for PG
162 measurements – rather it collates data from existing measurement sites and converts them into
163 a common format which is accessible to the wider research community. Presently the

164 GloCAEM dataset focuses on recent data, and many of the measurement sites are relatively
165 new with only a few years of data so far; however data are available back to 2005 for some
166 sites.

167

168 ***2.2 Parameters measured***

169 In terms of atmospheric electricity parameters, the GloCAEM dataset focuses principally on
170 measurements of PG as this is the most commonly measured quantity due to the relatively large
171 number of commercially-available sensors. The PG is present globally and is typically $\sim 100\text{V/m}$
172 in clear air during fair weather conditions at sea level, with larger values in polluted and non fair
173 weather conditions. PG is influenced by many factors including local meteorological influences,
174 dust and aerosol concentrations (e.g. Yair et al, 2016), global thunderstorm activity through the
175 GEC (e.g. Rycroft et al, 2000), space weather events (e.g. Marcz 1997; Harrison et al, 2013; De
176 et al, 2013) and changes in the ionisation rate from radon (e.g. Lopes et al, 2015), cosmic ray
177 changes (Mateev and Vellinov, 1992), and artificial ionisation sources (e.g. Takeda et al, 2011;
178 Fewes et al, 2002; Matthews et al, 2010), and changes in local site characteristics such as
179 variable electrical shielding effects of surrounding trees (Williams et al 2005) or buildings. Biotic
180 factors, such as vegetation and animal activity have thus far not been considered, yet have
181 been recognised to also affect local PG measurements. At any site the dominant changes in
182 the PG are likely to arise from local meteorological changes; therefore, it is important to
183 understand how various phenomena such as the local wind regime, rainfall, cloud, fog and
184 aerosol influence the measurement of PG (e.g. Deshpande and Kamra, 2001; Minamoto and
185 Kadokura, 2011; Bin et al, 2012; Harrison and Nicoll, 2018; Gurmani et al, 2018). Consequently
186 the GloCAEM dataset provides meteorological measurements in the form of: pressure,
187 temperature, relative humidity (RH), wind direction, wind speed, rainfall, global solar irradiance,
188 diffuse solar irradiance, visibility, sunshine duration and cloud base height. Although these
189 measurements are not available at every site, they are provided wherever and whenever

190 possible. The inclusion of a number of solar radiation and cloud measurements is to enable
191 different criteria to be explored in identifying fair weather conditions, since this aspect of data
192 selection (Harrison and Nicoll, 2018) is key for GEC studies. The GloCAEM dataset also allows
193 the study of different types of phenomena which cause perturbations in PG (such as
194 precipitation effects), which, for the purpose of GEC studies, can be averaged out; regular
195 systematic variations, however, must be dealt with in other ways. Aerosol-related effects on PG
196 can be both transient (e.g. short timescale effects from space weather), and systematic (e.g. the
197 sunrise effect, differences between weekdays and weekends, seasonal effects). These are
198 discussed more fully in section 3.2.

199

200 ***2.3 Instrumentation***

201 The PG has historically been measured by a number of different methods. These have included
202 potential probes, in which the potential on a conductor equalises with the potential of the
203 surrounding air and any subsequent changes in potential on the probe follow variations in PG
204 (e.g. Chalmers, 1967). Burning fuses, water droppers or radioactive probes have been
205 implemented to increase the conductivity of the air surrounding the probe to allow faster
206 equalisation rates (Israel, 1970). This technique is still employed at several of the GloCAEM
207 measurement stations, including Swider, Poland and Nagycenk, Hungary (Marcz et al, 2001),
208 where long time series of measurements are available. One of the main limitations of the
209 potential probe method is its slow time response, which is typically on the order of tens of
210 seconds depending on the method of equalisation employed. An alternative method is to use an
211 electric field mill, which allows much faster measurements (up to around 100Hz), and versions
212 which are robust to all meteorological conditions are available. An electric field mill typically
213 consists of a horizontal electrode, which is alternately exposed and shielded from the
214 atmospheric electric field. As the electrode is exposed to the electric field, a charge is induced
215 on the electrode, the magnitude of which is proportional to the field (e.g. Chubb, 2010; chapter 6

216 in MacGorman and Rust, 1998). This is measured with an electrometer, and phase sensitive
217 detection. Figure 1 shows some of the electric field mill sensors used at the various GloCAEM
218 sites. Technical details of the sensors are described fully as separate metafiles on the
219 GloCAEM project website ([https://glocaem.wordpress.com/introduction/project-partners-and-
220 measurement-sites/](https://glocaem.wordpress.com/introduction/project-partners-and-measurement-sites/)). This file also includes information on the height of the field mill sensors
221 above ground (which typically varies between 1 m and 3 m between sites). A full list of the
222 various field mill types used at the GloCAEM sites is given in table 1. It should be noted that
223 even though potential probe measurements are in use at some of the GloCAEM sites, only the
224 digitised PG measurements from field mills are currently included in the database.

225

226 PG measurements are recorded at a variety of sampling rates at the different GloCAEM sites
227 (from 2 Hz to 25 Hz), therefore to ensure consistency between sites, GloCAEM data have been
228 processed to report data at 1 second and 1 minute averages, in different data files. The
229 provision of data with different temporal resolution is intended to allow easier analysis of
230 phenomena which occur on a variety of timescales, without always having to download vast
231 amounts of data. It is important to point out that the absolute value of PG measured by a field
232 mill is affected both by calibration of the sensor and the physical environment surrounding the
233 sensor. Metal masts or guy lines distort the electric field, modifying the PG which is measured.
234 Thus, for PG measurements from different sites to be comparable, they must be standardised to
235 an open situation (such as flush with the ground surface, or compared with measurements from
236 a horizontal passive wire antenna), to remove the distorting effects. See e.g. Appendix in
237 Harrison and Nicoll, 2018 for more details. Field mill calibrations and site correction factors (to
238 account for the distortion of the electric field around the field mill mounting mast or nearby
239 buildings, are applied to data from some of the GloCAEM sites. Details of correction factors and
240 calibrations against other sensors are provided in the metafiles on the GloCAEM project website
241 (<https://glocaem.wordpress.com/introduction/project-partners-and-measurement-sites/>). Since

242 not all PG measurements in the GloCAEM database have been corrected for site distortion
243 factors, it is generally not meaningful to compare absolute PG measurements between all the
244 different sites. PG values with respect to the mean value at each site are therefore often
245 discussed throughout this paper to address this issue.

246

247 **2.4 Measurement sites**

248 At present the GloCAEM dataset comprises PG data from seventeen different locations ranging
249 from Poland in the north to Antarctica in the south. Figure 2 shows a map of the various
250 measurement sites which include ten different countries and four continents. Table 1 provides a
251 detailed description of the measurement sites in the GloCAEM dataset, and as with the
252 instrumentation information, the specifics of each site are included as a separate metafile on the
253 GloCAEM project website ([https://glocaem.wordpress.com/introduction/project-partners-and-
254 measurement-sites/](https://glocaem.wordpress.com/introduction/project-partners-and-measurement-sites/)). The sites include flat terrain in rural locations, mountainous regions, ice
255 shelves, deserts and rooftop locations in city centres. Whilst traditionally many of these site
256 locations would be avoided for atmospheric electricity research, the aim of GloCAEM is to
257 provide access to data for a wide range of related research purposes. For example: although
258 the PG may be enhanced as a result of the distortion caused by mountains, measurements in
259 such locations can provide information about boundary/exchange layer transitions (as well as in
260 cloud measurements) as these sites often move in and out of such layers as their altitude varies
261 (e.g. Israel, 1957; Kamogawa et al, 2015; Yaniv et al, 2017). PG measurements in city centre
262 locations can provide information on aerosol and pollution transport (e.g. Silva et al, 2016) and
263 desert measurements can provide valuable insights into dust electrification processes (e.g. Yair
264 et al, 2016; Yaniv et al, 2016; Esposito et al, 2016; Katz et al 2018).

265

266 Although the type of surface and surrounding orography influences the PG measurement, so
267 too does its geographical location in terms of the typical meteorological conditions that the site

268 experiences. Figures 3 and 4 show an example of differences in site climatology between
269 Graciosa, Azores - an island location in the North Atlantic Ocean - and Panská Ves - a
270 continental location in the Czech Republic. Although the median values of PG at both locations
271 for the year of 2016 are similar (80V/m at Graciosa, 49 V/m at Panská Ves²) the difference in
272 variability, and the range of PG values (from Figure 4) is obvious. This is mostly due to
273 climatological differences (in particular rainfall) between the two mid-latitude sites. This is
274 particularly true in the summer months, when Panská Ves experiences a relatively large number
275 of convective events compared to Graciosa, which causes large variability in the PG. It therefore
276 follows that Panská Ves is a better site for the study of convective activity, but Graciosa is likely
277 to be more suited to fair weather measurements which is required for study of the GEC. Greater
278 variability is expected in the Panská Ves data due to aerosol/conductivity variations that are
279 inherent at inland continental stations compared to the relatively clean oceanic air at the island
280 location of Graciosa. Thus the inclusion of different types of measurement locations in the
281 GloCAEM dataset will allow the study of many different types of phenomena of both local and
282 global origins.

283

284 **3. Analysis of GloCAEM PG data**

285 **3.1 Diurnal variations at GloCAEM sites**

286 One of the key parameters in global atmospheric electricity research is the diurnal variation in
287 PG on fair weather (FW) days. This is due to the fact that, in the absence of local influences,
288 the diurnal variation in PG is known to follow closely the diurnal variation in global thunderstorm
289 and shower cloud area, which together are understood to drive the global circuit. This result was
290 first established by Mauchly, (1921; 1923) and Whipple (1929) using the pioneering
291 measurements of the *Carnegie* research ship (e.g. Harrison, 2013). The characteristic shape of

² It should be noted that a site correction factor has only been applied to the data from Panská Ves and not Graciosa therefore the absolute values of PG are not directly comparable between the two sites.

292 this variation found by the Carnegie scientists, with a principal minimum around 03 UT and
293 principal maximum around 19 UT, is known as the Carnegie curve. Measurement sites which
294 exhibit a daily PG variation which is very similar to the Carnegie curve are often said to be
295 globally representative and hence, in principle can provide a method of monitoring the global
296 variation of the GEC from a single site measurement³. Analysis of the diurnal variation in PG
297 conditions has been performed for all of the GloCAEM sites. Since meteorological data is so far
298 available at only some of the GloCAEM sites - and hence true FW conditions cannot be
299 explicitly identified - the PG is selected for non-disturbed conditions on the basis of the PG
300 values only. This is based on the fact that non fair weather conditions (such as rainfall and high
301 winds) tend to produce large (as well as negative values of PG) (e.g. Bennett and Harrison,
302 2007). This approach may also remove situations in which the conductivity is low (e.g. during
303 high aerosol concentration events), which will produce abnormally large PG values, which would
304 not be detected by selection of meteorological conditions alone. Thus, what are considered
305 non-disturbed values of PG are selected individually for each site by only considering positive
306 PG values in the inner 80% of the distribution of PG values. This approach ensures that any
307 outliers in the PG distribution are removed from further analysis.

308

309 Figure 5 shows the percentage of non-disturbed periods (in black) for 9 of the GloCAEM sites
310 for each month of 2016. As expected, there is a large range between sites in the proportion of
311 non-disturbed values. For example, the maximum percentage of non-disturbed PG values in
312 any one month is 92% for Evora (EVO) (Oct 2016), whilst the minimum occurs for Xanthi (XAN)
313 at only 14% (March 2016). For the 5 sites with no missing data in 2016, Graciosa (GRA) has
314 the highest proportion (78%) of non-disturbed periods during the year, with Studenec (STU)
315 (33%) the least. There is also a seasonal effect evident at some sites, for example at Reading

³ Here we regard the “Carnegie curve” as the harmonic description of the undisturbed day PG data during Cruise 7 of the Carnegie provided by the Carnegie Institution (and re-analysed by Harrison 2013). Other secondary sources (e.g. Israel (1970)) differ slightly.

316 (RDG) and Swider (SWI), which are both mid-latitude sites and subject to an increased number
317 of non-fair weather conditions during winter months than summer. Such information can be
318 used to assess the most suitable GloCAEM sites for GEC studies, as well as what time of year
319 (if any) analysis should be focused on to increase the proportionality of non-disturbed data
320 available.

321
322 The average diurnal variation for non-disturbed values of PG during 2016 is shown for 15 of the
323 GloCAEM sites in Figure 6, alongside the Carnegie curve (red dashed line). Sites are combined
324 according to whether their diurnal variation in PG contains a single maximum, similar to the
325 Carnegie Curve, or two maxima (as assessed by eye). Because many of the sites are not
326 absolutely calibrated, comparison of absolute PG values cannot be undertaken: instead, the
327 sites' data are given as the percentage of the PG with respect to the median value for each site.
328 Median PG values before and after non-disturbed selection are shown in Table 2. Five of the
329 GloCAEM sites are shown to have a single maximum; however, the remaining ten sites
330 demonstrate evidence of substantial local effects (particularly following sunrise), with a double
331 peak in PG evident. This is to be expected as the majority of sites are continental and relatively
332 close to major population centres where aerosol pollution is abundant and responds to
333 atmospheric mixing. This so called "sunrise effect" has been observed at a variety of locations
334 (e.g. Marshall et al, 1996) and is generally thought to be related to mixing of the near-surface
335 electrode layer (which is an accumulation of positive charge next to the negatively charged
336 Earth's surface). At the majority of sites with two daily maxima, the first maximum is
337 proportionally smaller than the second, with the exception of Xanthi, Greece, where the morning
338 maximum is 30% larger than the evening one (Kastelis & Kourtidis, 2016). Such local
339 influences complicate any potential GEC analysis, but PG measurements from such sites will
340 provide valuable information on pollution and aerosol content of air and methods of minimising
341 the effects of such aerosols are discussed in section 3.2.

342

343 Of the sites which exhibit a single maximum, three of these are in mountainous locations with
344 altitudes above 2000 m. Although such sites may be subject to Austausch effects around
345 sunrise which can cause anomalously high values of PG due to turbulent and convective mixing
346 (e.g. Israel, 1957; Marshall et al., 1999; Yaniv et al, 2017), their high altitudes mean that they
347 are often above the polluted boundary layer and so can more readily detect GEC signals,
348 although this is not always the case. The presence of a Carnegie-like oscillation at Graciosa
349 (Azores); and Halley (Antarctica) is also not surprising as these are both relatively “clean” sites,
350 as Graciosa is located on a small island in the middle of the Atlantic Ocean, and Halley is on the
351 Brunt Ice Shelf. One explanation for the differences in the timings of the peak in the curve in
352 Figure 6 (a) may be related to the latitudinal and longitudinal distribution of the various
353 GloCAEM sites, where proximity to the major thunderstorm regions of the Americas, and the
354 African and Asian continents may influence the shape of the diurnal variation (e.g. Kamra et al,
355 1994). It should, however, be noted that there is disagreement in the literature as to whether or
356 not this phenomena occurs (particularly in regard to theoretical model results), and if so on what
357 time scale effects are evident.

358

359 Although there is considerable spread in the times of the maxima of the diurnal curves, the
360 minima in Figure 6 (regardless of whether the sites have single or double maxima) are generally
361 consistent at around 03-05 UT, similar to the Carnegie curve. Figure 7 demonstrates this by
362 showing the difference between the PG and Carnegie curve as a function of universal time (UT)
363 for sites with similar latitudes (and therefore similar times of day). The GloCAEM dataset
364 therefore supports the idea that the early morning UT hours are well suited to detecting global
365 circuit signals (as, e.g. suggested by Märcz, 1997), and even sites which demonstrate
366 considerable local influences during the day such as Xanthi should therefore not be discounted
367 from such analysis. In general, the time period from 21-06 local time (LT) is when local sources

368 of variability are less dominant and is therefore when the most globally representative times will
369 occur at the different GloCAEM sites.

370

371 **3.2 Influence of pollution**

372 The double maxima behaviour in the diurnal variation of PG in Figure 6 (b) is indicative of local
373 influences on PG and is typically related to anthropogenic pollution and seasonal effects.
374 Sources of particulate pollution can include local traffic, domestic heating, cooking or industry.
375 Even in Antarctica, which is typically a “clean” environment, diesel generators used to power
376 scientific bases can be a source of significant aerosol. The increased aerosol typically acts to
377 reduce the electrical conductivity, causing an associated increase in PG as expected from
378 Ohm’s Law when J_c is constant. The additional peak in the diurnal PG curve often appears
379 around sunrise, when the planetary boundary layer (PBL) is shallow (typically less than 1km)
380 and pollution sources from traffic and domestic heating and cooking are substantial. Previous
381 work (e.g. Sheftel et al 1994; Israelsson, & Tammet, 2001; Silva et al, 2014) has noted a
382 difference in PG between weekdays and weekends when traffic levels and industrial pollution
383 sources are often decreased. Such analysis can be applied to the GloCAEM sites to investigate
384 the effects of anthropogenic pollution at some of the sites which display a double diurnal
385 variation. Figure 8 shows boxplots of non-disturbed PG on weekdays (Monday to Friday) and
386 weekends (Saturday and Sunday) for Reading, Evora, Tripura and Xanthi (which all have
387 double maxima in their diurnal curves) using data from 2016. Typically, the weekday PG is
388 larger than that at weekends, for example, by up to 9% at Tripura, but only 2% at Evora. All
389 differences between weekday and weekend PG are statistically significant at the 5% level, with
390 the exception of Evora. The 5% increase in Reading PG during weekdays can be attributed to
391 increased pollution since Latha and Highwood (2006) reported a clear decrease in PM10
392 concentration during weekends compared to weekdays at Reading ($17 \mu\text{g m}^{-3}$ during weekdays
393 and $15 \mu\text{g m}^{-3}$ during weekends). They also noted an increase in PM10 through Monday to

394 Thursday, and decrease from Friday to Sunday, which also demonstrates that pollution
395 dispersal timescales will also play an important role in controlling PG. Although such a
396 difference between weekday and weekend PG supports the concept that a site may be affected
397 by anthropogenic pollution, further investigation is required to properly characterize this
398 contribution.

399

400 Air pollution often exhibits an annual cycle with maxima in winter and minima in summer due to
401 the annual variation in emissions (e.g. more use of domestic heating in winter and, in urban
402 areas, less traffic during holiday periods). The variation in convection and PBL height
403 throughout the seasons (which controls the distribution of aerosol particles near the surface)
404 also determines the magnitude of the effect of pollution on PG. Figure 9(a) shows the monthly
405 mean values of PG for Reading for weekends and weekdays. There is a clear seasonal cycle
406 with increased PG in winter (months 12 to 2) versus summer (months 5 to 8), which is most
407 pronounced in the weekday PG. This is likely to be related to traffic and regional industrial
408 production being at its greatest during weekdays, and coinciding with shallow boundary layer
409 depths during the winter months. The maximum of PG in the winter months at Reading follows
410 a similar winter maximum to that reported by Everett (1868) using instrumentation installed at
411 Kew, London, by Lord Kelvin.. Contrasting this with PG data from Graciosa⁴ (Figure 9 (b)),
412 which is a primarily clean air site (Lopes et al, 2017), both weekday and weekend PG values
413 maximize during the summer months. Measurements of aerosol optical depth at Graciosa
414 (Logan et al, 2014, not shown here) show a maximum aerosol number concentration (for 3-10
415 μm particles) during winter and spring, which is generally related to high wind speeds which
416 generate sea spray (this is the only substantial source of aerosol particles at Graciosa during
417 these months (Logan et al, 2014)). This seasonal dependence is opposite to the seasonal

⁴ No site correction factor has been applied to the Graciosa PG data therefore it is not meaningful to compare the absolute value of PG to other sites.

418 variation in PG, suggesting a negligible effect of the sea spray on the PG. This, and the fact
419 that the seasonal variability in the GEC predicts a NH summer maximum in PG, as is evident at
420 Graciosa, supports the interpretation of Graciosa as a clean air site and more suitable for GEC
421 measurements than urban locations.

422

423 Despite a number of the GloCAEM sites being influenced by local pollution it is possible to
424 select periods of the year when local influences are minimized. Figure 10 shows the diurnal
425 variation in PG at Reading for both winter and summer months, compared with the Carnegie
426 diurnal variation in PG. During the winter months, there is a single maximum (~15 UT), whereas
427 during the summer, a double maxima is present (at 06 and 19 UT), which is characteristic of the
428 mean diurnal variation at Reading when the average is taken over the whole year. As is also
429 demonstrated in Figure 9(a), the magnitude of the PG during the winter months is larger than in
430 the summer, consistent with Everett (1868) – most likely due to the increase in aerosol
431 emissions from domestic heating and trapping of this aerosol by a shallow PBL. The reduced
432 variability in PBL height during winter (due to diminished convection) therefore leads to more
433 quiescent meteorological conditions which results in a more stable diurnal variation in PG, and
434 the disappearance of the morning maximum peak. It therefore follows that many of the
435 GloCAEM sites which are affected by local sources of variability will inevitably have periods
436 (such as during the winter months) which are less dominated by local effects and are therefore
437 more globally representative. This was demonstrated by Harrison et al (2011) who, using data
438 from December months when more quiescent conditions prevailed, detected a GEC response to
439 the El Nino-Southern Oscillation (ENSO) in PG data from Shetland, UK.

440

441 ***3.3 Average diurnal behaviour across multiple sites***

442 There is considerable interest in whether a global PG dataset can provide information on daily
443 variability within the global circuit (and therefore a proxy for global electrified clouds), which is

444 generally not possible by using PG from one site due to interference from local sources of
445 variability. This has been suggested to have potential applications for simple monitoring of
446 global temperatures due to the dependence of the GEC on surface temperature and global
447 thunderstorm activity (e.g. Price, 1993).

448

449 To investigate this, Figure 11 shows (in black) the variation in PG on two individual days
450 averaged into hourly values across six of the GloCAEM sites, compared with the Carnegie
451 curve (in red). Only sites with more than 10 months of data for 2016, and which exhibit
452 Carnegie-like curves on at least one individual day, are considered for this analysis. Even so,
453 the averaging approach should act to minimise any local influences on PG such as fluctuations
454 in aerosol concentration. There is clear similarity between the heavily averaged Carnegie curve
455 and the daily averages across the GloCAEM sites, particularly in the timings of the maxima.
456 The differences evident in the GloCAEM curves between Figure 11 (a) and (b) also warrant
457 further investigation into the source of the much lower PG values in Figure 11(b) (possibly due
458 to a decrease in global thunderstorm activity) that day, as well as the detection of the secondary
459 peak at 0900UT which is normally due to thunderstorm activity in Asia (potentially due to
460 increased activity in this area on this day). Curves possessing a similar shape to the Carnegie
461 curve, with a minimum in the early morning hours and single maximum around 19 UT (assessed
462 by eye), were observable on ~ 25% of days in 2016 using this averaging method. This is a
463 substantial increase in the number of days from any single site in the GloCAEM database. This
464 therefore demonstrates that averaging across multiple sites may well improve the statistics of
465 observing Carnegie-like signals on a day-to-day basis.

466

467 ***3.4 Seasonal variations in PG at GloCAEM sites***

468 Establishing the exact nature of the seasonality in the GEC has not been a simple task due to
469 interference of local influences on PG which, themselves have their own seasonal variations

470 (e.g. boundary layer heights and aerosol concentrations) (Adlerman and Williams, 1996;
471 Williams, 2009). The few fair weather PG measurements from the Carnegie during the northern
472 hemisphere summer months on its main cruise (e.g. Harrison 2013), as well as the
473 geographically varying Carnegie PG measurements have also added to the complexity as
474 proximity to major thunderstorm regions (e.g. Kamra et al, 1994), and their seasonal variation
475 may be an additional factor. It has therefore required measurements from clean air sites such
476 as Antarctica (e.g. Burns et al, 1995; 2005; 2012; 2017) to confirm that the GEC has a northern
477 hemisphere (NH) summer maxima, in agreement with the summer maxima in global lightning
478 activity.

479

480 PG measurements from Amundsen-Scott South Pole station (Reddell et al, 2004), Vostok
481 (Burns et al, 2005), and Concordia, all in Antarctica, have proved invaluable in establishing the
482 seasonal variation in the GEC, but maintaining PG instrumentation in such harsh polar
483 environments makes long term measurements difficult. To investigate the suitability of current
484 GloCAEM sites for seasonal GEC monitoring, Figure 12 shows seasonally averaged values of
485 the diurnal variation in non-disturbed PG at three of the GloCAEM sites which exhibit single
486 peaks in their diurnal PG curves – Graciosa, Halley and CAS2. Although typically only two
487 years of data are included for each site, which is not ideal for seasonal studies, differences can
488 be seen in the shape of the curves between seasons and times of the maxima and minima. The
489 existence of a small peak around 06-09 UT is evident at Halley (which varies seasonally), but
490 not at Graciosa or CAS2 which exhibit pronounced minima at this time. This is particularly
491 prevalent at CAS2, and may be attributed to the lack of influence of the Asian thunderstorm
492 generator (due to the large distances involved between Asia and Argentina), which typically
493 maximises around 06-09 UT (Tacza et al, 2014). It should also be noted that Halley and CAS2
494 are southern hemisphere sites, and CAS2 in particular is likely to be influenced by the nearby
495 South American thunderstorm generator region, which has a maximum thunderstorm output in

496 DJF (southern hemisphere summer), which may lead to the highest maxima in PG (128% with
497 respect to the mean) being observed in this season. The high latitude of Halley also suggests
498 that the PG there may be subject to additional variations present on a diurnal scale, caused by
499 the ionospheric interaction with the solar wind (known as cross-polar cap variations (e.g.
500 Weimer, 1996)). This additional diurnal variation would be superposed with the GEC variation,
501 and is known to lead to differences in the timing of minima and maxima at certain Antarctic sites
502 (e.g. Vostok and South Pole station (Burns et al, 2012)). The westward Antarctic location of
503 Halley, on the Brunt Ice Shelf, means that such effects are likely to be small, and only likely an
504 issue during disturbed solar periods, but a full analysis of the Halley data is required to remove
505 such effects.

506

507 Figure 13 investigates the variations in the timing of the maxima and minima in the diurnal
508 variations of PG for each of the three GloCAEM sites as a function of season and compares
509 them with the timings of the PG maxima observed by the Carnegie (data from Harrison, 2013)
510 and at Vostok (data from Burns et al, 2005). As is seen, for the timing of the maxima, the
511 Carnegie and Vostok timings show an increase from NH winter through to summer, with
512 maximum in the summer months (JJA), which results from a summer maximum in global
513 thunderstorm activity in the NH. The three GloCAEM sites show a similar increasing trend from
514 NH winter, but display a maximum in spring (MAM). There may be several explanations for this
515 including a lack of data (typically less than 2 years of measurements for each site) and the
516 proximity of sites to major regions of thunderstorms and electrified shower clouds, which may
517 dominate over global influences at certain times of the year. In terms of the timing of the
518 minimum, all sites (with the exception of CAS2, which does not have a dominant minimum in
519 DJF) show the same trend with a spring maximum. The better agreement between sites in
520 terms of the trend in the time of the minimum is likely related to the fact that there is less
521 influence of local variability on the PG during the early morning hours (as demonstrated in

522 Figure 7). It is evident therefore that although some of the GloCAEM sites show promise for
523 GEC monitoring, more data are required to fully assess their suitability.

524

525 **4. Discussion and future directions**

526 The GLOCAEM network aims to archive PG data generated from a variety of measurement
527 types and locations around the globe, which can be utilized to study different scientific
528 phenomena related to atmospheric electricity. Table 3 summarises some of these phenomena
529 and provides initial recommendations of the GloCAEM sites most suited for such analysis. The
530 most widely studied topic in fair weather atmospheric electricity has historically been that of the
531 GEC, which typically requires long time series of PG measurements in fair weather conditions, in
532 unpolluted locations. Although several of the GLOCAEM sites promise to be suitable for such
533 studies, detailed analysis is yet to be undertaken, providing further insight into the data available,
534 its analysis and its future reporting. Measurement of the GEC from surface PG measurements is
535 difficult because of local influences such as aerosol variations. Despite the continental nature of
536 most of the GloCAEM sites, this paper has however demonstrated that even sites which are
537 subject to variable influences from e.g. local sources of aerosol, can demonstrate some global
538 representability with careful selection of data. This includes restricting data seasonally (e.g.
539 winter periods which show less atmospheric mixing), using weekend data only (less sources of
540 anthropogenic pollution), and focusing on periods of the day which are subject to less local
541 influences, such as 2100-0600 LT. The ability to monitor the daily GEC variability through the
542 diurnal variation in PG on individual days is highly desirable, because of its relationship with
543 global temperature changes (e.g. Williams, 1992; 1994). The GloCAEM database thus provides
544 the opportunity to fully test whether averaging many simultaneous PG measurements from
545 around the globe (as in Figure 11) can provide a more robust determination of the GEC on daily
546 timescales than from any one site, which will only encounter FW conditions intermittently.

547

548 Although at the moment GloCAEM archives only PG data, the format of the data files has been
549 created such that inclusion of other atmospheric electricity variables such as air-Earth
550 conduction current (J_c) and conductivity (σ) measurements can be included in the future. In
551 order to more completely represent the GEC, a similar network of σ and J_c sensors will be
552 required, but the difficulties associated with automating measuring these parameters robustly
553 has prevented this so far. Scope also exists for the inclusion of historical datasets, and the
554 global coverage of sites is expected to be extended in 2019 with the inclusion of further PG
555 datasets.

556

557 **5. Summary**

558 This paper summarises the features of a new dataset for global PG measurements, GloCAEM,
559 encompassing four continents and 17 different measurement sites. The work presented is very
560 likely to be one of the largest single analysis of global PG data using multiple datasets
561 simultaneously, which demonstrates the usefulness of a dataset with identical data formatting
562 for each site. The variety of different site locations and characteristics contained within the
563 GloCAEM database now means that a number of scientific problems related to atmospheric
564 electricity can be more easily investigated, these include GEC studies, ENSO and climate
565 effects, space weather influences on atmospheric electricity, charging of dust, snow, fog, cloud
566 and aerosols, interactions between PG and biological activity, and turbulent transport of space
567 charge to name a few, and recommendations are given here on the sites most suitable for such
568 analysis. Of the preliminary GEC analysis performed, the GloCAEM dataset is demonstrated to
569 contain several sites which show promise for the study of the GEC (primarily Graciosa (Azores),
570 Halley (Antarctica) and CAS (Argentina)). The averaging of PG during non-disturbed conditions
571 from a number of GloCAEM sites on a daily basis is also demonstrated to produce globally
572 representative signals, potentially leading to the ability to study day to day variations in the
573 GEC, which has so far proved difficult from a single site. The creation of the GloCAEM database

574 therefore represents a major step forward in the synthesis which has previously limited
575 atmospheric electricity research, yet provides access to central elements of the climate system.

576

577

578 **Acknowledgements**

579 The authors would like to thank all of the GloCAEM project partners and their colleagues who
580 have provided data for the database (list of names is found at:
581 <https://glocaem.wordpress.com/introduction/project-partners-and-measurement-sites/>). Wendy
582 Garland at CEDA has been key to the design and implementation of the GloCAEM database.
583 This work is funded by a NERC International Opportunities Fund grant NE/N013689/1 to KAN.
584 KAN also acknowledges a NERC Independent Research Fellowship (NE/L011514/1 and
585 NE/L011514/2). The authors also wish to acknowledge EU COST action CA15211 Atmospheric
586 Electricity Network: coupling with the Earth system, climate and biological systems. The
587 GloCAEM data catalogue can be found at:
588 <http://catalogue.ceda.ac.uk/uuid/bffd0262439a4ecb8fadf0134c4a4a41>. The contribution of
589 J. Bór was supported by the National Research, Development and Innovation Office, Hungary-
590 NKFIH, project ID K115836. J.-P. Raulin and J. Tacza acknowledge the support of CAPES
591 and the Air Force Office of Scientific Research, Air Force Material Command, USAF under
592 Award No. FA9550-16-1-0072.

593

594

595

596 **Table captions**

597

598 Table 1. Details of the GloCAEM measurement sites and electric field mill instrumentation
599 deployed.

600

601 Table 2. Details of PG characteristics for the 17 GloCAEM sites for 2016 (except CGR which
602 only has PG values for 2017). Values are calculated from 10 minute averages and FW PG
603 values are selected as those between 0 V/m and 80% of the total PG distribution.

604

605 Table 3. Recommendations of GloCAEM sites most suited to the study of a variety of scientific
606 phenomena in atmospheric electricity research.

607

608 **Figure Captions**

609

610 Figure 1. Example of different types of electric field mill sensors used in the GloCAEM network.
611 (a) JCI 131F field mill (Chilworth UK) at Graciosa, Azores; (b) CS110 field mill (Campbell
612 Scientific) at the Wise Observatory, Mitzpe Ramon, Israel; (c) EFM 100 field mill (Boltek) at
613 Nagycenk, Hungary.

614

615 Figure 2. Site locations within the GloCAEM dataset.

616

617 Figure 3. Time series of PG values during 2016 at (a) Graciosa, Azores, (b) Panská Ves, Czech
618 Republic. Data are 10 minute mean values and the y axis has been restricted to +/- 2000 V/m
619 on both plots.

620

621 Figure 4. Comparison of PG histograms for (a) Graciosa, Azores; and (b) Panská Ves, Czech
622 Republic, (for 10 minute mean values and plotted within a range of ± 500 V/m).

623

624 Figure 5. Strip chart of percentage of non-disturbed PG values for each month for GloCAEM
625 sites with more than 10 months of data in 2016 (using 10 minute mean values of PG). Black
626 shows percentage of non-disturbed PG, grey disturbed PG, and red denotes no data available
627 during that time period. Percentages are given with respect to total data available for that
628 month at a specific site. Site abbreviation codes are given in Table 1.

629

630 Figure 6. Mean undisturbed diurnal variation in PG for 2016 for (a) GloCAEM sites with a single
631 peak in the diurnal curve and (b) double peak, plotted as a percentage of the median PG for
632 each site. Data are selected for non-disturbed conditions using only positive PG values and PG
633 values less than the 80th decile of the distribution for each individual site (using 10 min average

634 values), with a smoothing spline applied. (a) Carnegie (red), Graciosa (purple), Halley (orange),
635 CAS2 (M) (blue), Mt Hermon (M) (black), Aragats (M) (grey) (b) Carnegie (red), Studenec
636 (black), Reading (blue), Panská Ves (purple), Xanthi (grey), Tripura (cyan), Swider (orange),
637 Evora (pink), Bristol Langford (green), Mitzpe Ramon (grey dashed), Nagycenk (blue dashed).
638 (M) indicates mountainous sites.

639

640 Figure 7. Boxplot of difference between non-disturbed diurnal average PG and Carnegie PG
641 during 2016 (expressed as a percentage difference) for Reading, Bristol Langford, Mitzpe
642 Ramon, Xanthi, Evora, Swider, Nagycenk, Studenec and Panská Ves, as a function of time of
643 day. Only sites which are in similar latitudinal regions are included, and mountain sites are also
644 excluded due to Austausch effects. The edges and line in the centre of each box show the
645 upper and lower quartiles, and the median and whiskers extend to 1.5 times the interquartile
646 range. Individual points represent outliers.

647

648 Figure 8. Boxplots of non-disturbed 10 minute mean PG values on weekdays (Monday to
649 Friday) and weekends (Saturday and Sunday) using data from 2016. Measurements sites are
650 (a) Reading, (b) Evora, (c) Tripura, (d) Xanthi. The upper and lower box boundaries and central
651 horizontal show the upper and lower quartiles, and the median respectively. Notches around the
652 median indicate the 95% confidence limits, with median and p-values shown on the plot.
653 Outliers are not shown.

654

655 Figure 9. Median monthly variation in non-disturbed PG for weekday (grey) and weekend
656 (black) PG (calculated from 10 minute mean PG values). (a) Reading (using data from 2010 to
657 2018) and (b) Graciosa (using data from 2015 to September 2017).

658

659 Figure 10. Mean undisturbed diurnal variation in PG for Reading during (a) winter (December,
660 January, February – DJF) and (b) summer (June, July, August – JJA) in black. PG data is
661 averaged from 10 minute mean values and covers 2010-2018. Red shows the annual average
662 Carnegie variation in PG.

663

664 Figure 11. Diurnal variation in PG on individual days (a) 20th April 2016 and (b) 15th May 2016,
665 averaged from the sites at Reading, Graciosa, Evora, CAS2, Nagycenk, Panská Ves (black,
666 with a cubic smoothing spline applied, with smoothing parameter of 0.4). Only non-disturbed
667 values of PG are included and values are first normalised individually with respect to the median
668 for each site and then averaged together (using the median value). Averages are hourly
669 averages taken from 1 minute PG data. The red line is the normalised Carnegie PG.

670

671 Figure 12. Mean diurnal variation in non-disturbed PG as a function of season at the most
672 globally representative GloCAEM sites of Graciosa (data from 2015 to Sept 2017), Halley (data
673 from 2015 to 2017) and CAS2 (Argentina) (data from 2016 to 2018). (a) December, January,
674 February (DJF), (b) March, April May (MAM), (c) June, July, August (JJA) and (d) September,
675 October, November (SON). The time of the PG maximum at each site is shown by the vertical
676 dashed lines. Curves are computed from 10 minute mean values.

677

678 Figure 13. Time of the (a) maximum and (b) minimum in diurnal variation in non-disturbed PG
679 as a function of season from various sites including the Carnegie, Vostok Antarctica; and the
680 GloCAEM sites of Graciosa (data from 2015 to Sept 2017), Halley (data from 2015 to 2017) and
681 CAS2 (Argentina) (data from 2016 to 2018). Carnegie data is obtained from Harrison (2013)
682 and Vostok data from Burns et al (2005). Vostok has more data points than the other sites as
683 seasonal PG averages are reported over 2 month periods (Burns et al, 2005), unlike the other
684 sites where averages are calculated over 3 month periods.

685 **References**

686

687 Adlerman, E.J., Williams, E.R., 1996. Seasonal variation of the global electrical circuit. J.
688 Geophys. Res. 101 (D23), 29679–29688.

689

690 Bennett, A.J., Harrison, R.G., 2007. Atmospheric electricity in different weather conditions.
691 Weather, 62(10), 277-283.

692

693 Berliński, J., Pankanin, G., Kubicki, M, 2007. Large scale monitoring of troposphere electric
694 field. Proceedings of the 13-th ICAE, Beijing, China, 1, 124-126.

695

696 Bin, X., Hua, H., Xiao-Yan, Y. Ye-Guang,B., Qing-Hua, L.,2012, The study of meteorological
697 effects and time variations of the fair weather atmospheric electric field near ground in YBJ,
698 Tibet, Acta Phys. Sin, 61(17), 175203, doi:10.7498/aps.61.175203

699

700

701 Burns, G. B., Hesse, M. H., Parcell, S. K., Malachowski, S., & Cole, K. D., 1995, The geoelectric
702 field at Davis station, Antarctica. Journal of Atmospheric and Terrestrial Physics, 57(14), 1783-
703 1797.

704

705 Burns, G. B., Frank-Kamenetsky, A. V., Troshichev, O. A., Bering, E.A., Reddell, B. D., 2005.
706 Interannual consistency of bi-monthly differences in diurnal variations of the ground-level,
707 vertical electric field. J.Geophys. Res., (D10) 110.

708

709 Burns, G. B., Tinsley, B. A., Frank-Kamenetsky, A. V., Troshichev, O. A., French, W. J. R., &
710 Klekociuk, A. R., 2012, Monthly diurnal global atmospheric circuit estimates derived from Vostok

711 electric field measurements adjusted for local meteorological and solar wind influences. Journal
712 of the Atmospheric Sciences, 69(6), 2061-2082.

713

714 Burns, G. B., Frank-Kamenetsky, A. V., Tinsley, B. A., French, W. J. R., Grigioni, P.,
715 Camporeale, G., & Bering, E. A., 2017, Atmospheric global circuit variations from Vostok and
716 Concordia electric field measurements. Journal of the Atmospheric Sciences, 74(3), 783-800.

717

718 Chalmers, J.A., 1967. Atmospheric Electricity. 2nd Edition, Pergamon press, Oxford, UK.

719

720 Chilingarian, A., Chilingaryan, S., & Reymers, A., 2015. Atmospheric discharges and particle
721 fluxes. J.Geophys. Res.Space Physics, 120 (7), 5845-5853.

722

723 Chilingarian, A., 2018, Long lasting low energy thunderstorm ground enhancements and
724 possible Rn-222 daughter isotopes contamination, Physical Review D, 98, 022007.

725

726 Chubb J., 2010. An introduction to electrostatic measurements. Nova Science Publishers, New
727 York

728

729 De, S.S., Bandyopadhyay, B., Paul, S., Haldar, D.K., Bose,M., Kala, D., & Guha, G., 2013,
730 Atmospheric electric potential gradient at Kolkata during solar eclipse of 22 July 2009, Indian
731 Journal of Radio & Space Physics, 42, 251-258.

732

733 Deshpande, C.G., Kamra, A.K., 2001. Diurnal variations of the atmospheric electric field and
734 conductivity at Maitri, Antarctica. J.Geophys. Res. Atmospheres 106 (D13) 14207-14218.

735

736 Esposito, F., Molinaro, R., Popa, C. I., Molfese, C., Cozzolino, F., Marty, L., et al., 2016. The
737 role of the atmospheric electric field in the dust-lifting process. *Geophysical Research Letters*,
738 43(10), 5501-5508.

739

740 Everett, J. D. (1868). XI. Results of observations of atmospheric electricity at Kew Observatory,
741 and at King's College, Windsor, Nova Scotia. *Philosophical Transactions of the Royal Society of*
742 *London*, 158, 347-361.

743

744 Fews, A.P., Wilding, R.J., Keitch, P.A., Holden, N.K., Henshaw, D.L., 2002. Modification of
745 atmospheric DC fields by space charge from high-voltage power lines. *Atmospheric Research*
746 63, 271–289, doi:10.1016/S0169-8095(02)00041-8

747

748 Gurmani, S.F., Ahmad, N., Tacza, J., Iqbal, T., 2018. First seasonal and annual variations of
749 atmospheric electric field at a subtropical station in Islamabad, Pakistan. *Journal of Atmospheric*
750 *and Solar-Terrestrial Physics*, 179, 441-449. DOI: 10.1016/j.jastp.2018.09.011

751

752 Harrison, R.G., Joshi, M., & Pascoe, K., 2011. Inferring convective responses to El Niño with
753 atmospheric electricity measurements at Shetland. *Environmental Research Letters*, 6(4),
754 044028.

755

756 Harrison, R.G., 2013. The Carnegie curve. *Surveys in Geophysics*, 34(2), 209-232.

757

758 Harrison, R.G., Nicoll, K.A., McWilliams, K.A., 2013. Space weather driven changes in lower
759 atmosphere phenomena. *Journal of Atmospheric and Solar-Terrestrial Physics*, 98, 22-30.

760

761 Harrison, R.G., Nicoll, K.A., 2018. Fair weather criteria for atmospheric electricity
762 measurements, *Journal of Atmospheric and Solar-Terrestrial Physics*, in press.
763

764 Israël, H. 1957. Atmospheric electric and meteorological investigations in high mountain ranges.
765 Alpen-Programm 1954-57, Final Report to Contract No. AF 61, 514-640.
766

767 Israël, H. 1970. *Atmospheric Electricity*. (2 volumes), Israel Program for Scientific Translations,
768 Jerusalem.
769

770 Israelsson, S., Tammet, H., 2001. Variation of fair weather atmospheric electricity at Marsta
771 Observatory, Sweden, 1993–1998. *Journal of atmospheric and solar-terrestrial physics*, 63(16),
772 1693-1703.
773

774 Kamogawa, M., Suzuki, Y., Sakai, R., Fujiwara, H., Torii, T., Kakinami, Y., et al., 2015. Diurnal
775 variation of atmospheric electric field at the summit of Mount Fuji, Japan, distinctly different from
776 the Carnegie curve in the summertime. *Geophysical Research Letters*, 42(8), 3019-3023.
777

778 Kamra, A. K., Deshpande, C. G., & Gopalakrishnan, V., 1994. Challenge to the assumption of
779 the unitary diurnal variation of the atmospheric electric field based on observations in the Indian
780 Ocean, Bay of Bengal, and Arabian Sea. *Journal of Geophysical Research: Atmospheres*, 99
781 (D10), 21043-21050.
782

783 Kastelis, N., Kourtidis, K., 2016. Characteristics of the atmospheric electric field and correlation
784 with CO₂ at a rural site in southern Balkans. *Earth, Planets and Space*, 68(1), 3.
785

786 Katz, S., Yair, Y., Price, C., Yaniv, R., Silber, I., Lynn, B., & Ziv, B., 2018. Electrical properties of
787 the 8–12th September, 2015 massive dust outbreak over the Levant. *Atmospheric Research*,
788 201, 218-225.

789

790 Kelvin, Lord., 1860. *Atmospheric Electricity*, Royal Institution Lecture, *Papers on Electrostatics*
791 *and Magnetism*, 208-226

792

793 Krider, E. P., 1989. Electric field changes and cloud electrical structure. *Journal of Geophysical*
794 *Research: Atmospheres*, 94(D11), 13145-13149.

795

796 Latha, K. M., Highwood, E. J., 2006. Studies on particulate matter (PM10) and its precursors
797 over urban environment of Reading, UK. *Journal of Quantitative Spectroscopy and Radiative*
798 *Transfer*, 101(2), 367-379.

799

800 Logan, T., Xi, B., Dong, X., 2014. Aerosol properties and their influences on marine boundary
801 layer cloud condensation nuclei at the ARM mobile facility over the Azores. *Journal of*
802 *Geophysical Research: Atmospheres*, 119(8), 4859-4872.

803

804 Lopes, F., Silva, H.G., Bárias, S., Barbosa, S.M., 2015. Preliminary results on soil-emitted
805 gamma radiation and its relation with the local atmospheric electric field at Amieira (Portugal),
806 *Journal of Physics: Conference Series* 646, 012015, doi:10.1088/1742-6596/646/1/012015

807

808 Lopes, F.M., Silva, H.G., Bennett, A.J., & Reis, A. H. (2017). Global Electric Circuit research at
809 Graciosa Island (ENA-ARM facility): First year of measurements and ENSO influences. *Journal*
810 *of Electrostatics*, 87, 203-211.

811

812 Lucas, G.M., Thayer, J.P., Deierling, W., 2017. Statistical analysis of spatial and temporal
813 variations in atmospheric electric fields from a regional array of field mills. *Journal of*
814 *Geophysical Research: Atmospheres*, 122(2), 1158-1174.

815

816 MacGorman D.R., Rust W.D., 1998. *The electrical nature of storms*. Oxford University Press,
817 New York

818

819 Márcz, F., 1997, Short-term changes in atmospheric electricity associated with Forbush
820 decreases, *Journal of Atmospheric and Solar-Terrestrial Physics* , 59 (9), 975-982

821

822 Márcz, F., Horváth, J., Bencze, P., Sántori, G., Bór, J., 2001. Simultaneous measurements of the
823 atmospheric electric potential gradient at nagycenk observatory by means of two individual
824 equipments, *Acta Geodaetica et Geophysica Hungarica*, 36 (3), 269-278

825

826 Marshall, T. C., Rust, W. D., Stolzenburg, M., Roeder, W. P., & Krehbiel, P. R., 1999, . A study
827 of enhanced fair-weather electric fields occurring soon after sunrise. *Journal of Geophysical*
828 *Research: Atmospheres*, 104(D20), 24455-24469.

829

830 Mateev, L.N., Vellinov P.I., 1992, Cosmic ray variations effects on the parameters of the global
831 atmospheric electrical circuit, *Advances in Space Research*, 12 (10), 353-356.

832

833 Matthews, J.C., Ward, J.P., Keitch, P.A., Henshaw, D.L., 2010. Corona ion induced atmospheric
834 potential gradient perturbations near high voltage power lines, *Atmospheric Environment*, 44
835 (39), 5093-5100, doi:10.1016/j.atmosenv.2010.09.007

836

837 Mauchly S.J., 1921, Note on the diurnal variation of the atmospheric electric potential gradient.
838 Phys Rev, 18:161–162
839

840 Mauchly S.J., 1923, On the diurnal variation of the potential gradient of atmospheric electricity.
841 Terr Magn, 28:61–81

842 Minamoto, Y., Kadokura A., 2011, Extracting fair-weather data from atmospheric electric-field
843 observations at Syowa Station, Antarctica, Polar Science, 5, (3), 313-318.
844

845 Michnowski, S. , 1998, Solar wind influences on atmospheric electricity variables in polar
846 regions. *Journal of Geophysical Research: Atmospheres*, 103(D12), 13939-13948.
847

848 Nicoll, K.A., Measurements of atmospheric electricity aloft, 2012. *Surveys in Geophysics*, 33, 5,
849 991-1057
850

851 Nicoll, K.A., Harrison, R.G., 2016. Stratiform cloud electrification: comparison of theory with
852 multiple in-cloud measurements *Q. J. R. Meteor. Soc.* 142, 700, 2679-2691. DOI:
853 10.1002/qj.2858
854

855 Nicoll, K.A., Harrison, R.G., 2014. Detection of lower tropospheric responses to solar energetic
856 particles at mid-latitudes, *Physical Review Letters*, 112, 225001.
857

858 Price, C., 1993. Global surface temperatures and the atmospheric electrical circuit. *Geophysical*
859 *Research Letters*, 20(13), 1363-1366.
860

861 Raulin, J. P., Tacza, J., Macotela, E., Fernandez, G., 2014. A new South America electric field
862 monitor network. *Sun Geosphere*, 9(1-2), 111-114.

863

864 Reddell, B. D., Benbrook, J. R., Bering, E. A., Cleary, E. N., Few, A. A., 2004. Seasonal
865 variations of atmospheric electricity measured at Amundsen-Scott South Pole Station. Journal
866 of Geophysical Research: Space Physics, 109 (A9).

867

868 Rycroft, M. J., Israelsson, S., Price, C., 2000. The global atmospheric electric circuit, solar activity
869 and climate change, Journal of Atmospheric and Solar-Terrestrial Physics, 62, 1563-1576.

870

871 Sheftel, V. M., Chernyshev, A. K., Chernysheva, S. P., 1994. Air conductivity and atmospheric
872 electric field as an indicator of anthropogenic atmospheric pollution. Journal of Geophysical
873 Research: Atmospheres, 99(D5), 10793-10795.

874

875 Popov I. B., Shvarts Ya. M., Sokolenko L., 2008. Atmospheric electricity measurements on a
876 ground meteorological network of Federal Hydrometeorology and Environmental Monitoring
877 Service (Roshydromet). TECO-2008 - WMO Technical Conference on Meteorological and
878 Environmental Instruments and Methods of Observation, St. Petersburg, Russian Federation,
879 27-29 November 2008, accessible at
880 [https://www.wmo.int/pages/prog/www/IMOP/publications/IOM-96_TECO-](https://www.wmo.int/pages/prog/www/IMOP/publications/IOM-96_TECO-2008/P1(50)_Shvarts_Russian_Federation.pdf)
881 [2008/P1\(50\)_Shvarts_Russian_Federation.pdf](https://www.wmo.int/pages/prog/www/IMOP/publications/IOM-96_TECO-2008/P1(50)_Shvarts_Russian_Federation.pdf).

882

883 Silva, H. G., Conceição, R., Melgão, M., Nicoll, K., Mendes, P. B., Tlemçani, M., et al., 2014.
884 Atmospheric electric field measurements in urban environment and the pollutant aerosol weekly
885 dependence. Environmental Research Letters, 9(11), 114025.

886

887 Silva, H, Conceição, R, Khan, A, Matthews, J, Wright, M, Collares-Pereira, M & Shallcross, D,
888 2016. Atmospheric electricity as a proxy for air quality: Relationship between potential gradient
889 and pollutant gases in an urban environment. *Journal of Electrostatics*, 84., 32-41.
890

891 Smirnov, S., 2014. Reaction of electric and meteorological states of the near-ground
892 atmosphere during a geomagnetic storm on 5 April 2010. *Earth, Planets and Space*, 66(1), 154.
893

894 Tacza, J., Raulin, J. P., Macotela, E., Norabuena, E., Fernandez, G., Correia, E., et al., 2014. A
895 new South American network to study the atmospheric electric field and its variations related to
896 geophysical phenomena. *Journal of Atmospheric and Solar-Terrestrial Physics*, 120, 70-79.
897

898 Takeda, M., Yamauchi, M., Makino, M., & Owada T., 2011. Initial effect of the Fukushima
899 accident on atmospheric electricity. *Geophysical Research Letters* 38, L15811,
900 doi:10.1029/2011GL048511.
901

902 Tammet, H., 2009. A joint dataset of fair-weather atmospheric electricity. *Atmospheric*
903 *Research*, 91(2), 194-200.
904

905 Tinsley, B. A., Burns, G. B., & Zhou, L., 2007. The role of the global electric circuit in solar and
906 internal forcing of clouds and climate. *Advances in Space Research*, 40(7), 1126-1139.
907

908 Vergeiner, I., 1972. Comments on: On fine structure and control of vertical aerosol exchange
909 between 700 m and 3000 m by R. Reiter, R. Sládkovič, and W. Carnuth. *Archiv für*
910 *Meteorologie, Geophysik und Bioklimatologie, Serie A*, 21(1), 123-126.
911

912 Weimer, D. R., 1996. A flexible, IMF dependent model of high-latitude electric potentials having
913 “space weather” applications. *Geophysical Research Letters*, 23(18), 2549-2552.
914

915 Whipple F.J.W., 1929. On the association of the diurnal variation of the electric potential
916 gradient in fine weather with the distribution of thunderstorms over the globe. *Q. J. R. Meteorol.*
917 *Soc.* 55, 351–361
918

919 Williams, E.R., 1992. The Schumann resonance: A global tropical thermometer. *Science*,
920 256(5060), 1184-1187.
921

922 Williams, E. R., 1994, Global circuit response to seasonal variations in global surface air
923 temperature. *Monthly Weather Review*, 122(8), 1917-1929.
924

925 Williams, E.R., 2005. Lightning and climate: A review. *Atmospheric Research*, 76(1-4), 272-287.
926

927 Williams, E R, 2009. The global electrical circuit: A review, *Atmospheric Research*, 91(2–4),
928 140–152, doi:10.1016/j.atmosres.2008.05.018.
929

930 Williams, E., Markson, R., Heckman, S., 2005, Shielding effects of trees on the measurement of
931 the Earth's electric field: implications for secular variations of the global electrical circuit.
932 *Geophys. Res. Lett.* 32, L19810.
933

934 Wilson, C.T.R., 1921. Investigations on lightning discharges and on the electric field of
935 thunderstorms, *Philos. Trans. R. Soc. London, Ser. A*, 221, 73–115,
936 doi:10.1098/rsta.1921.0003.
937

938 Yair, Y., Katz, S., Yaniv, R., Ziv, B., Price, C., 2016. An electrified dust storm over the Negev
939 desert, Israel. Atmospheric Research, 181, 63-71.

940

941 Yaniv, R., Yair Y., Price, C., Katz, S., 2016. Local and global impacts on the fair weather
942 electric field in Israel. Atmospheric Research, 172-173, 119-125.

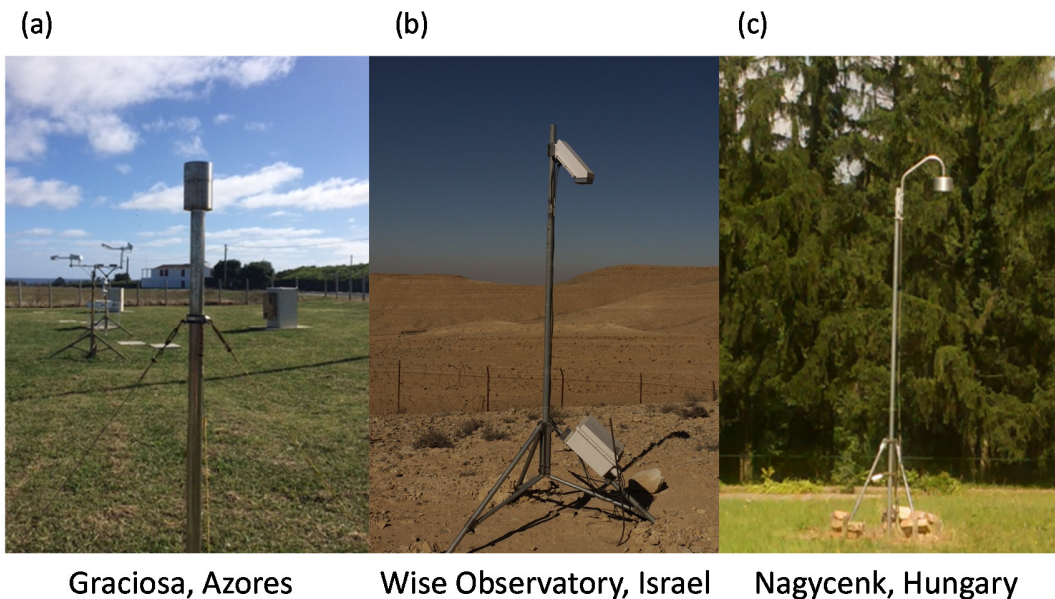
943

944 Yaniv, R., Yair, Y., Price, C., Mkrtchyan, H., Lynn, B., Reymers, A., 2017. Ground-based
945 measurements of the vertical E-field in mountainous regions and the “Austausch” effect.
946 Atmospheric Research, 189, 127-133.

947

948

949



Graciosa, Azores

Wise Observatory, Israel

Nagycenk, Hungary

950
951

952

Figure 1. Example of some of the different types of electric field mill sensors used in the

953

GloCAEM network. (a) JCI 131F field mill (Chilworth UK) at Graciosa, Azores; (b) CS110 field

954

mill (Campbell Scientific) at the Wise Observatory, Mitzpe Ramon, Israel; (c) EFM 100 field mill

955

(Boltek) at Nagycenk, Hungary.

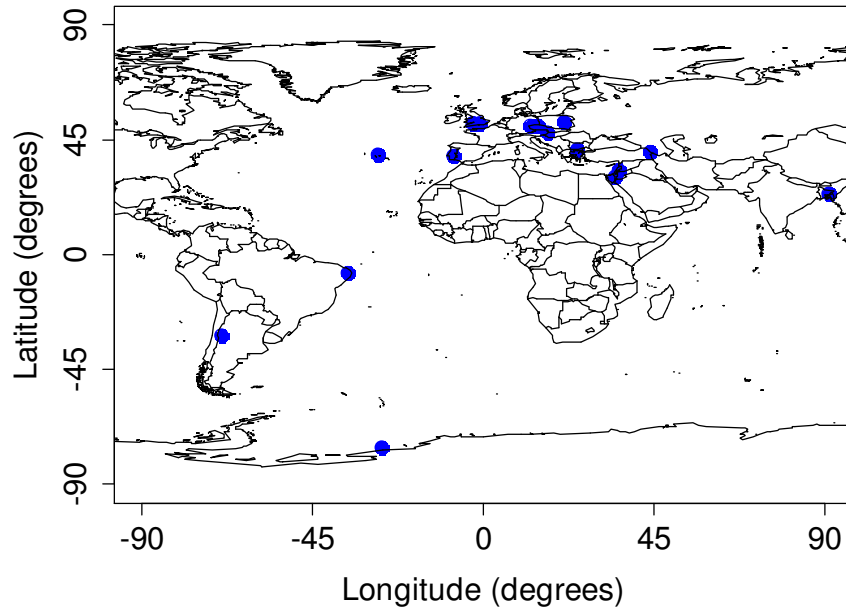
956

957

958

959

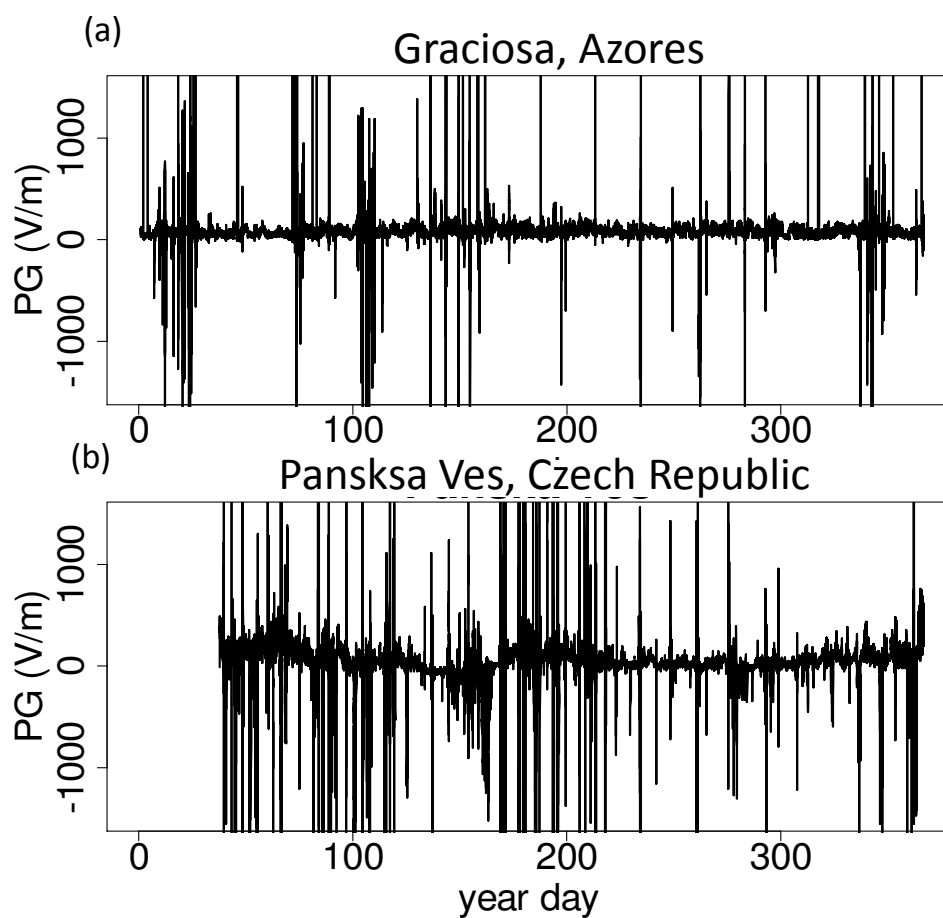
960



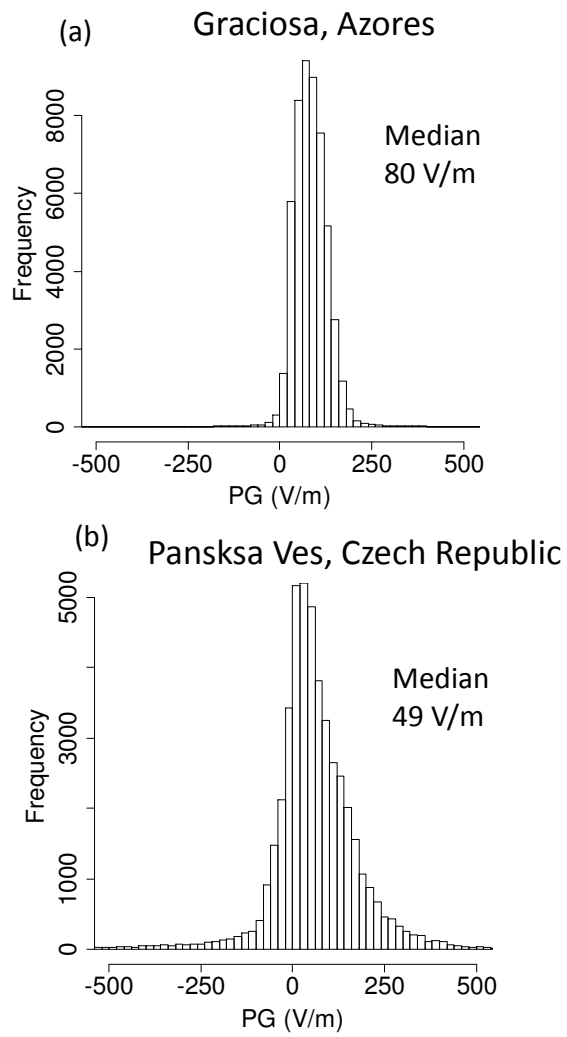
961
962 Figure 2. Map of measurement locations within the GloCAEM dataset.

Institute	Site	Site abbreviation	Country	Site type	PG instrument	Coordinates and altitude a.s.l
University of Reading	University of Reading	RDG	UK	Urban, grassy	JCI 131 Chilworth	51.44°N, 0.94°W 66 m
University of Reading	Halley research station	HAL	Antarctica	Ice shelf	JCI 131 Chilworth	75.58°S, 26.66°W 30 m
University of Bristol	At-Bristol Science Centre	BRISCI	UK	Urban (on 15m rooftop)	JCI 131F Chilworth	51.45°N, 2.60°W 45 m
University of Bristol	Langford School of Veterinary Sciences	BRILANG	UK	Rural, grassy	JCI 131F Chilworth	51.35°N, 2.78°W 23 m
Interdisciplinary Centre (IDC) Herzliya	Mount Hermon cosmic ray station	HER	Israel	Mountainous	Campbell CS110	33.30°N, 35.78°E 2050 m
Interdisciplinary Centre (IDC) Herzliya	Wise Astronomical Observatory, Mitzpe Ramon	RAM	Israel	Rural, desert	Campbell CS110	30.58°N, 34.75°E 875 m
Demokritos University of Thrace	Duth, Xanthi	XAN	Greece	Rural, grassy	Campbell CS110	41.15°N, 24.92°E 75 m
University of Evora	University of Evora	EVO	Portugal	Urban, grassy	JCI 141F Chilworth	38.57° N, 7.90° W 270 m
University of Evora	Graciosa, Azores	GRA	Portugal	Island, rural, grassy	JCI 131F Chilworth	39.09°N, 28.03°W 31 m
Yerevan Physics Institute	Aragats Space Environmental Center	ARA	Armenia	Mountainous (on 10 m rooftop)	Boltek EFM100	40.47°N, 44.18°E 3200 m
Polish Academy of Sciences	Swider Geophysical Observatory	SWI	Poland	Rural, grassy	Berlinski et al., ICAE, 2007	52.12°N, 21.24°E 96 m
Hungarian Academy of Sciences	MTA CSFK GGI Szechenyi Istvan Geophysical Observatory, Nagycenk	NCK	Hungary	Rural, grassy	Boltek EFM100	47.63°N, 16.72°E 153 m
Tripura University	Tripura University	TRI	India	Rural, grassy (on 14 m rooftop)	Boltek EFM100	23.76°N, 91.26°E 43 m
Academy of Sciences of Czech Republic	Studeneč,	STU	Czech Republic	Rural, grassy	Boltek EFM100	50.26°N, 12.52°E 712 m
Academy of Sciences of Czech Republic	Panska Ves	PAN	Czech Republic	Rural, grassy	Boltek EFM100	50.53°N, 14.57°E 315 m
Complejo Astronómico El Leoncito	Complejo Astronómico El Leoncito, San Juan	CAS2	Argentina	Mountainous	Boltek EFM100	31.8°S, 69.29°W 2483 m
Paraíba State University	Paraíba State University, Paraíba	CGR	Brazil	Scrubland (on 15 m rooftop)	Boltek EFM100	7.21°S, 35.92°W 550 m

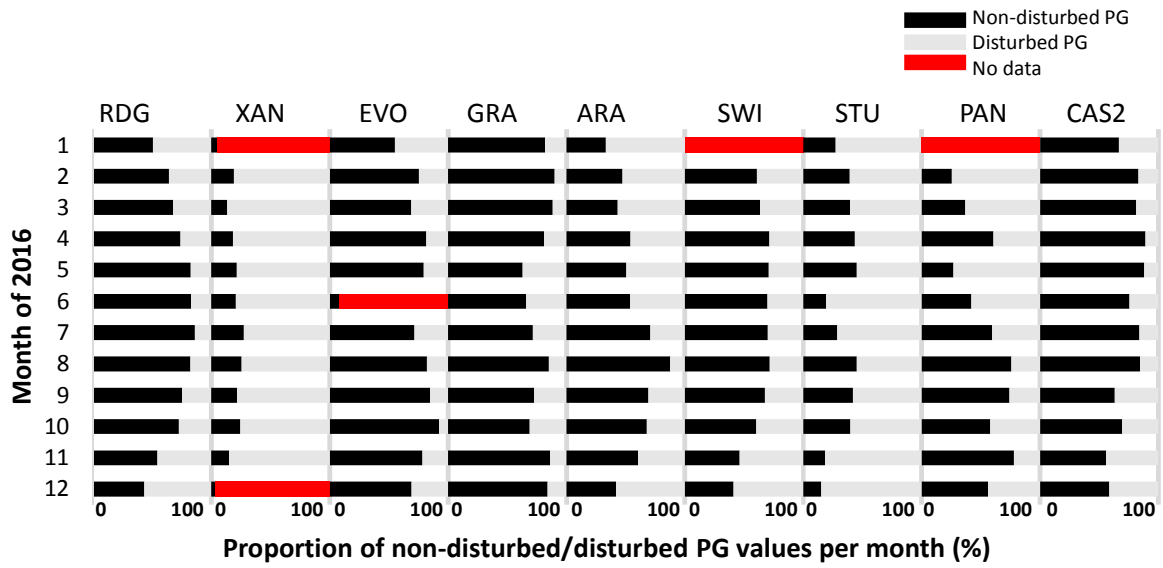
963
964 Table 1. Details of the GloCAEM measurement sites and electric field mill instrumentation
965 deployed.



966
 967 Figure 3. Time series of PG values during 2016 at (a) Graciosa, Azores, (b) Panská Ves, Czech
 968 Republic. Data are 10 minute mean values and the y axis has been restricted to +/- 2000 V/m
 969 on both plots.
 970

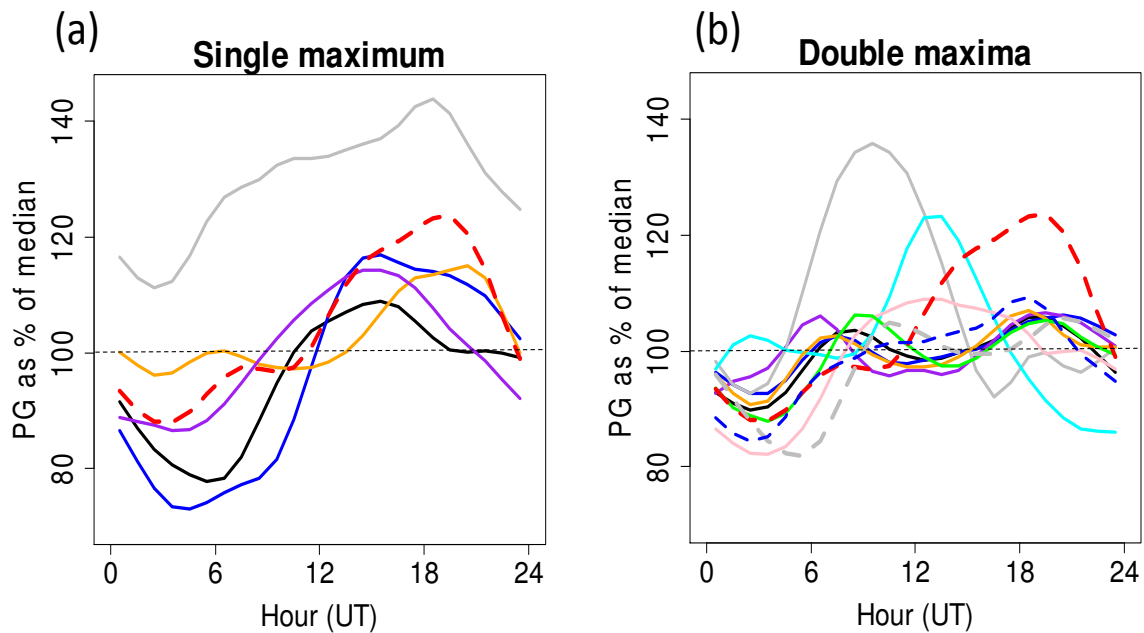


971
 972 Figure 4. Comparison of PG histograms for (a) Graciosa, Azores; and (b) Panská Ves, Czech
 973 Republic, (for 10 minute mean values and plotted within a range of ± 500 V/m).
 974



975
 976 Figure 5. Strip chart of percentage of non-disturbed PG values for each month for GloCAEM
 977 sites with more than 10 months of data in 2016 (using 10 minute mean values of PG). Black
 978 shows percentage of non-disturbed PG, grey disturbed PG, and red denotes no data available
 979 during that time period. Percentages are given with respect to total data available for that
 980 month at a specific site. Site abbreviation codes are given in Table 1.

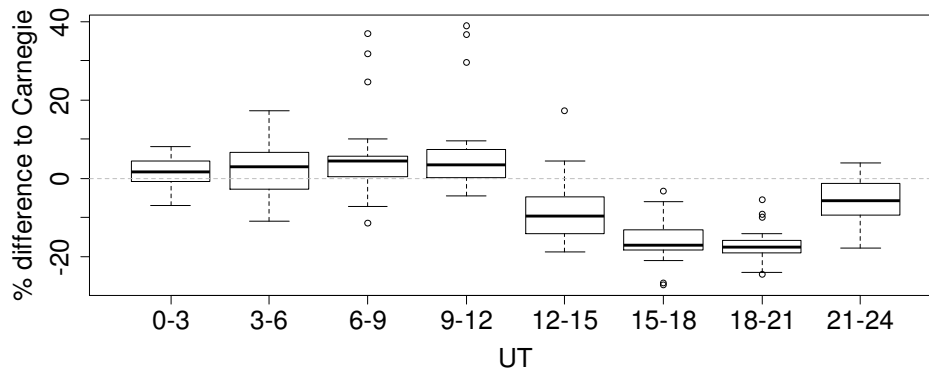
981
 982
 983
 984
 985
 986
 987
 988
 989



990
 991
 992 Figure 6. Mean undisturbed diurnal variation in PG for 2016 for (a) GloCAEM sites with a single
 993 peak in the diurnal curve and (b) double peak, plotted as a percentage of the median PG for
 994 each site. Data are selected for non-disturbed conditions using only positive PG values and PG
 995 values less than the 80th decile of the distribution for each individual site (using 10 min average
 996 values), with a smoothing spline applied. (a) Carnegie (red), Graciosa (purple), Halley (orange),
 997 CAS2 (M) (blue), Mt Hermon (M) (black), Aragats (M) (grey) (b) Carnegie (red), Studenec
 998 (black), Reading (blue), Panska Ves (purple), Xanthi (grey), Tripura (cyan), Swider (orange),
 999 Evora (pink), Bristol Langford (green), Mitzpe Ramon (grey dashed), Nagycenk (blue dashed).
 1000 (M) indicates mountainous sites.

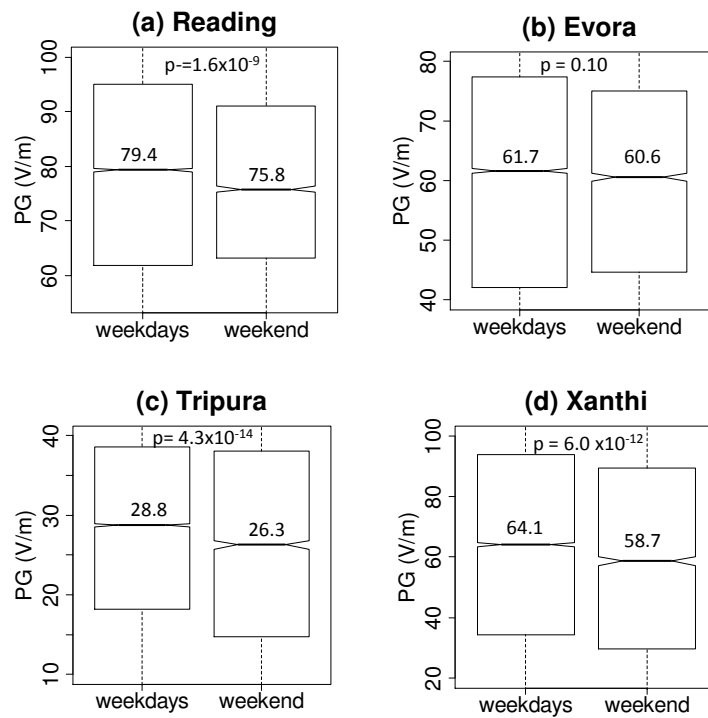
Site	Site abbreviation	All PG median (V/m)	All PG standard deviation (V/m)	Non-disturbed PG median (V/m)	Type of PG diurnal cycle	Number complete months of data
University of Reading	RDG	85	85	80	Double	12
Halley research station	HAL	69	272	65	Single	10
At-Bristol Science Centre	BRISCI	216	521	205	Insufficient data	7
Langford School of Veterinary Sciences	BRILANG	20	81	21	Double	8
Mount Hermon cosmic ray station	HER	245	558	233	Single (Mountain)	7
Wise Astronomical Observatory, Mitzpe Ramon	RAM	186	222	179	Double	8
Duth, Xanthi	XAN	68	520	63	Double	10
University of Evora	EVO	67	1203	64	Double	11
Graciosa	GRA	81	249	75	Single	12
Aragats Space Environmental Center	ARA	111	1367	115	Single (Mountain)	12
Swider Geophysical Observatory	SWI	273	431	259	Double	11
MTA CSFK GGI Szechenyi Istvan Geophysical Observatory, Nagycenk	NCK	167	652	154	Double	9
Tripura University	TRI	30	101	29	Double	9
Studeneč	STU	48	96	44	Double	12
Panska Ves	PAN	49	311	53	Double	11
CAS2	CAS2	431	1359	404	Single (Mountain)	11
CGR	CGR	195	336	184	Single	12 (for 2017)

1001
1002 Table 2. Details of PG properties for the 17 GloCAEM sites for 2016 (except CGR which only
1003 has PG values for 2017). Values are calculated from 10 minute averages and FW PG is
1004 selected on the basis of between 0 V/m and 80% of the total PG distribution.



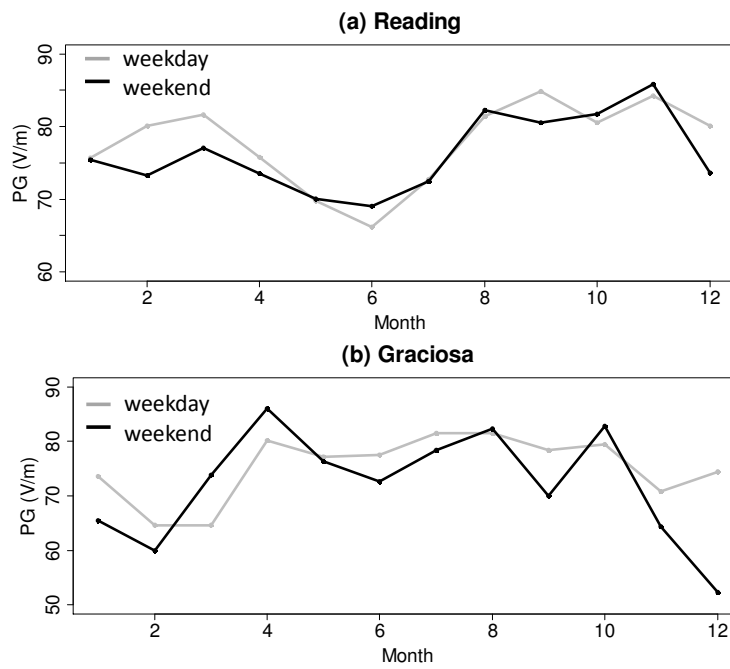
1005 Figure 7. Boxplot of difference between non-disturbed diurnal average PG and Carnegie PG
 1006 during 2016 (expressed as a percentage difference) for Reading, Bristol Langford, Mitzpe
 1007 Ramon, Xanthi, Evora, Swider, Nagycenk, Studenec and Panska Ves, as a function of time of
 1008 day. Only sites which are in similar latitudinal regions are included, and mountain sites are also
 1009 excluded due to Austausch effects. The edges and line in the centre of each box show the
 1010 upper and lower quartiles, and the median and whiskers extend to 1.5 times the interquartile
 1011 range. Individual points represent outliers.

1013
 1014
 1015
 1016



1017
 1018
 1019
 1020
 1021
 1022
 1023
 1024
 1025
 1026

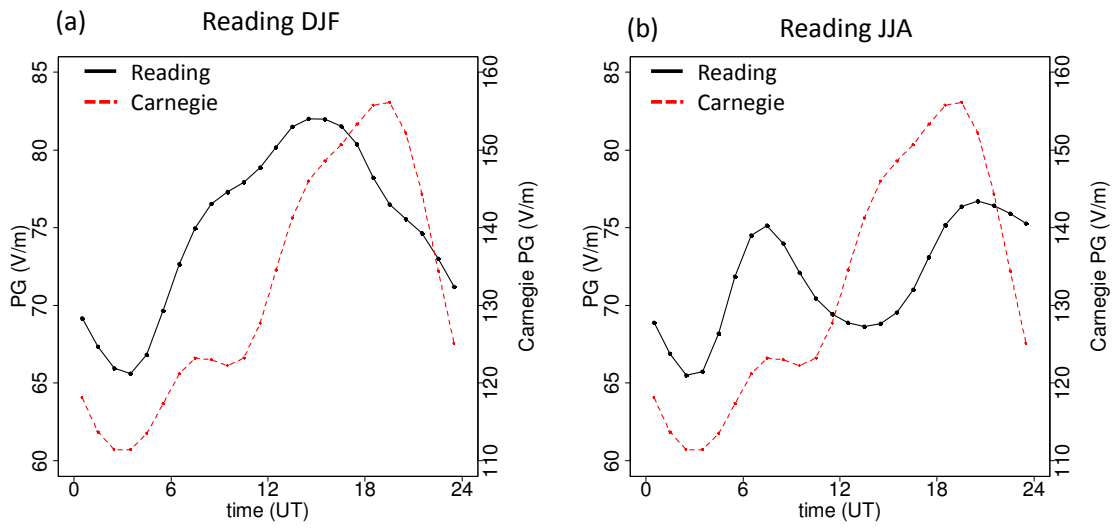
Figure 8. Boxplots of non-disturbed 10 minute mean PG values on weekdays (Monday to Friday) and weekends (Saturday and Sunday) using data from 2016. Measurements sites are (a) Reading, (b) Evora, (c) Tripura, (d) Xanthi. The upper and lower box boundaries and central horizontal show the upper and lower quartiles, and the median respectively. Notches around the median indicate the 95% confidence limits, with median and p-values shown on the plot. Outliers are not shown.



1027
1028
1029

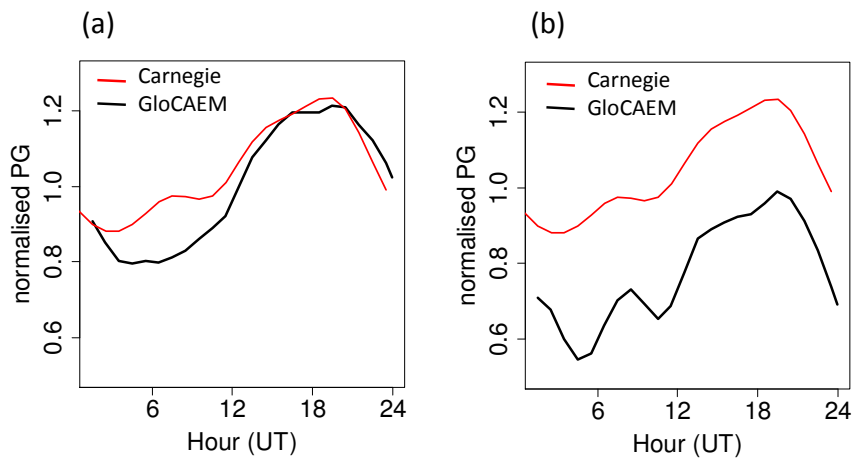
1030 Figure 9. Median monthly variation in non-disturbed PG for weekday (grey) and weekend
1031 (black) PG (calculated from 10 minute mean PG values). (a) Reading (using data from 2010 to
1032 2018) and (b) Graciosa (using data from 2015 to September 2017).

1033
1034
1035
1036
1037



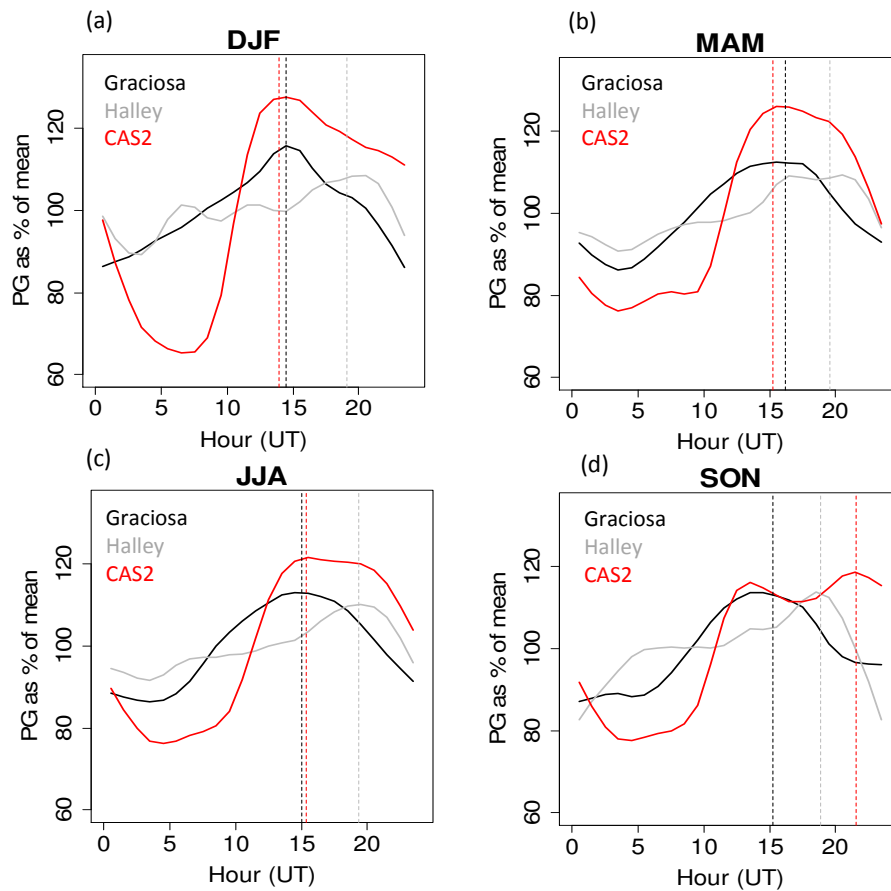
1038
 1039
 1040
 1041
 1042
 1043
 1044
 1045
 1046
 1047
 1048
 1049
 1050
 1051
 1052
 1053
 1054
 1055

Figure 10. Mean undisturbed diurnal variation in PG for Reading during (a) winter (December, January, February – DJF) and (b) summer (June, July, August – JJA) in black. PG data is averaged from 10 minute mean values and covers 2010-2018. Red shows the annual average Carnegie variation in PG.



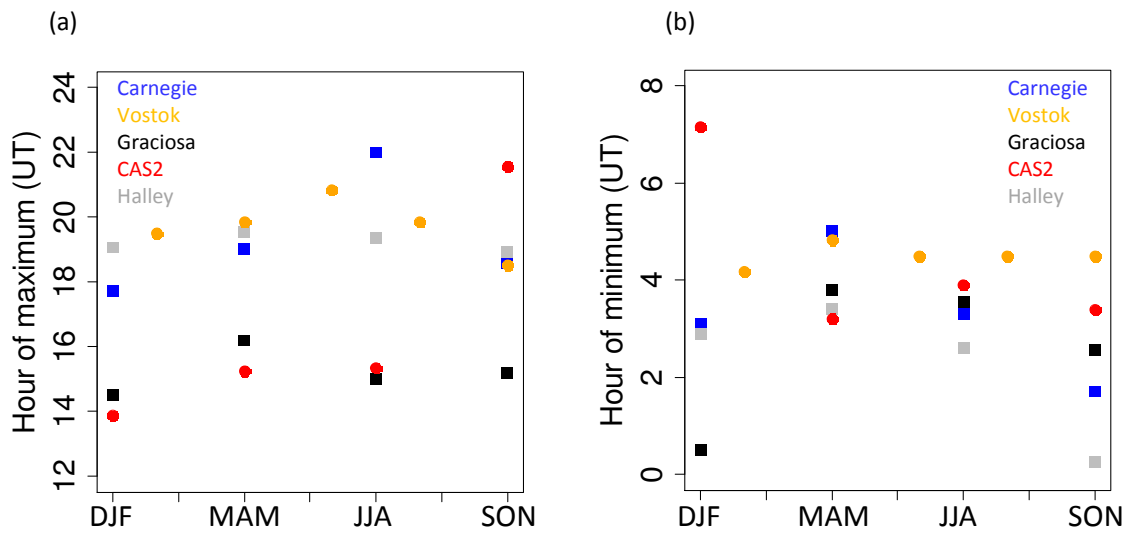
1056 Figure 11. Diurnal variation in PG on individual days (a) 20th April 2016 and (b) 15th May 2016,
 1057 averaged from the sites at Reading, Graciosa, Evora, CAS2, Nagycenk, Panská Ves (black,
 1058 with a cubic smoothing spline applied, with smoothing parameter of 0.4). Only non-disturbed
 1059 values of PG are included and values are first normalised individually with respect to the median
 1060 for each site and then averaged together (using the median value). **Averages are hourly**
 1061 **averages taken from 1 minute PG data.** The red line is the normalised Carnegie PG.

1063
 1064
 1065
 1066



1067
 1068 Figure 12. Mean diurnal variation in non-disturbed PG as a function of season at the most
 1069 globally representative GloCAEM sites of Graciosa (data from 2015 to Sept 2017), Halley (data
 1070 from 2015 to 2017) and CAS2 (Argentina) (data from 2016 to 2018). (a) December, January,
 1071 February (DJF), (b) March, April May (MAM), (c) June, July, August (JJA) and (d) September,
 1072 October, November (SON). The time of the PG maximum at each site is shown by the vertical
 1073 dashed lines. Curves are computed from 10 minute mean values.

1074
 1075



1076
 1077 Figure 13. Time of the (a) maximum and (b) minimum in diurnal variation in non-disturbed PG
 1078 as a function of season from various sites including the Carnegie, Vostok Antarctica; and the
 1079 GloCAEM sites of Graciosa (data from 2015 to Sept 2017), Halley (data from 2015 to 2017) and
 1080 CAS2 (Argentina) (data from 2016 to 2018). Carnegie data is obtained from Harrison (2013)
 1081 and Vostok data from Burns et al (2005). Vostok has more data points than the other sites as
 1082 seasonal PG averages are reported over 2 month periods (Burns et al, 2005), unlike the other
 1083 sites where averages are calculated over 3 month periods.

1084
 1085
 1086
 1087
 1088
 1089
 1090
 1091
 1092
 1093
 1094
 1095
 1096
 1097
 1098
 1099
 1100

Scientific Phenomenon	Best site for analysis
Global electric circuit	Graciosa, Halley, CAS2
El Nino (ENSO)	Graciosa
Thunderstorm electrification	Aragats
Stratiform cloud electrification	Reading, Swider
Aerosol and pollution	Reading, Tripura, Xanthi
Dust electrification	Mitzpe Ramon
Snow electrification	Halley, Mt Hermon, Aragats
Earthquakes	Evora, Xanthi
Austausch/boundary layer transition	Mt Hermon, Aragats

1101

1102 Table 3. Recommendations of GloCAEM sites most suited to the study of a variety of scientific

1103 phenomena in atmospheric electricity research.

1104

1105